

CASE FILE COPY

CONVECTION IN SKYLAB M512
EXPERIMENTS M551, M552
AND M553

PHASE B REPORT

July 1973

Lockheed

HUNTSVILLE RESEARCH & ENGINEERING CENTER

LOCKHEED MISSILES & SPACE COMPANY, INC.
A SUBSIDIARY OF LOCKHEED AIRCRAFT CORPORATION

HUNTSVILLE, ALABAMA

LOCKHEED MISSILES & SPACE COMPANY, INC.
HUNTSVILLE RESEARCH & ENGINEERING CENTER
HUNTSVILLE RESEARCH PARK
4800 BRADFORD DRIVE, HUNTSVILLE, ALABAMA

CONVECTION IN SKYLAB M512
EXPERIMENTS M551, M552
AND M553

PHASE B REPORT

July 1973

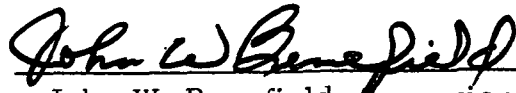
Contract NAS8-27015

Prepared for National Aeronautics and Space Administration
Marshall Space Flight Center, Alabama 35812


by

S. V. Bourgeois, Jr.

APPROVED:



John W. Benefield, Supervisor
Fluid Mechanics Section



J. S. Farrior
Resident Director

FOREWORD

This report summarizes the results of the Phase B portion of Contract NAS8-27015 for the 12-month period ending 15 July 1973. This effort was performed by the Lockheed-Huntsville Research & Engineering Center for NASA-Marshall Space Flight Center.

The NASA Contracting Officer's Representative (COR) for this study is Mr. T. C. Bannister, S&E-SSL-T. The NASA principal investigators for this study are Mr. R. M. Poorman (M551), S&E-ASTN-MM; Mr. J. R. Williams (M552), S&E-PT-M; and Mr. E. A. Hasemeyer (M553), S&E-PT-MWM.

CONTENTS

<u>Section</u>		<u>Page</u>
	FOREWORD	ii
1	INTRODUCTION AND SUMMARY	1
2	M551 EXPERIMENT	6
	2.1 Results	6
	2.2 Expected Low-G Variations	8
	2.3 Phase C Evaluations	10
	2.4 Conclusions and Summary	10
3	M552 EXPERIMENT	12
	3.1 Results	12
	3.2 Expected Low-G Variations	14
	3.3 Phase C Evaluations	14
	3.4 Conclusions and Summary	15
4	M553 EXPERIMENT	16
	4.1 Results	17
	4.2 Expected Low-G Variations	18
	4.3 Phase C Evaluations	19
	4.4 Conclusions and Summary	19
	REFERENCES	22
Appendixes		
A	Nominal Operating Conditions for the Skylab M512 Chamber	A-1
B	Detailed Analyses for the M551 Experiment	B-1
C	Detailed Analyses for the M552 Experiment	C-1
D	Detailed Analyses for the M553 Experiment	D-1

Section 1

INTRODUCTION AND SUMMARY

Under Contract NAS8-27015, Lockheed-Huntsville is analyzing Skylab Experiments M551 (Metals Melting), M552 (Exothermic Brazing), M553 (Sphere Forming), and M566 (Al-Cu Eutectic Growth). The primary objective is the study of convection in the molten metals and their attendant solidification theory. Particular attention is given to clarifying the effects of reduced gravity on molten metal flow and solidification.

Under Phase A of this contract, a ground-based study plan was prepared. A summary report (Ref. 1) was issued on this 10-week phase ending July 1972. The ground study program defined in Phase A is the subject of the present report. The Phase C portion of this contract will consist of a comparative analysis between Skylab I flight specimens and data versus those ground-based and KC-135 specimens and data already processed. The Phase C segment will continue through January 1974. The reporting of Phase B and Phase C results for the M566 experiments will each be delayed approximately three months because this experiment will be flown on Skylab IV.

This Phase B report is concerned specifically with the Metals Melting Experiment, the Exothermic Brazing Experiment, and the Sphere Forming Experiment to be performed in the M512 facility during the Skylab I mission of May-June 1973. These experiments are described briefly as follows:

M551 Metals Melting Experiment: Three sample disks, each containing three metal specimens of varying thicknesses, are to be rotated automatically at a controlled speed under an electron beam gun such that an electron beam weld seam is produced in the metal specimen. Disk materials include 2219 Aluminum, 321 Stainless Steel and tantalum. During the continuous weld portion of each disk, both full and partial penetration of the disk will be

achieved by having a constant power input but a varying disk thickness. For each disk, the continuous weld will be followed by a dwell portion. In the dwell portion of the weld, the disk will remain stationary while the electron beam impinges on a thick segment of the disk, thus creating a large molten pool. The electron beam will then be shut off and the pool will be allowed to solidify.

M552 Exothermic Brazing: A technique for joining stainless steel tubes will be tested in this experiment and the flow and solidification behavior of weightless molten braze alloys will be studied. The joining technique will use a solid mixture that produces heat by exothermic chemical reaction to braze sleeves over 0.75-inch diameter tubes, using a copper-silver-lithium braze alloy. A package containing four assemblies, each consisting of a tube with sleeve and preformed braze alloy surrounded by exothermic material, will be mounted in the M512 facility's vacuum chamber. The exothermic reactions in the four assemblies will be ignited in sequence and the whole package will be returned to earth for analysis.

M553 Sphere Forming Experiment: Twenty-eight 0.25-inch diameter spherical specimens will be cast using the electron beam gun as a heat source. The specimens will be initially supported on two wheels by a sting. After melting is completed, the spheres will then be separated from their stings and allowed to solidify while free-floating in the vacuum chamber. Specimens will consist of the following materials: pure nickel, Ni-1% Ag, Ni-30% Cu, and Ni-12% Sn.

The nominal operating conditions for the electron beam gun, braze units and the M512 vacuum chamber are given in Appendix A. This appendix also contains the updated convection sensitivity analysis for all the M512 experiments (M551, M552, M553 and M556).

For these particular Skylab experiments, the only significant difference between space and earth processing will be the lack of gravity. Other environmental factors which may also differ from earth processing are the vacuum, radiation, electromagnetic and thermal conditions.

Gravity has no direct effect on grain structure or other properties of solidified material. These properties are determined by the crystallization kinetics which are controlled by short-range intermolecular forces; i.e., the temperature and concentration at the fluid-solid interface. Gravity has not been shown to have any significant direct effect on these forces, but can affect solidification indirectly through its direct effect on fluid motion. The three major indirect effects of gravity on solidification are:

- Sedimentation
- Bouyancy-Induced Convection, and
- Hydrostatic Pressure.

In addition to these three very important indirect effects, the lack of gravity will also afford the study of a more direct effect — the opportunity to obtain homogeneous nucleation. The long free-float times potentially available in space processing applications will allow melts to cool and nucleate without the deleterious effects of container walls. Wall effects are usually very strong in nucleation phenomena and prevent large degrees of supercooling from being attained in terrestrial processing. The remaining indirect effects are explained further below.

Sedimentation: This effect may be significant whenever heterogeneous mixtures exist in fluids, such as in monotectic, dispersed-particle, or fiber-reinforced composite casting. The denser of the immiscible materials will tend to settle unless colloidal or electrostatic attractions interfere. Also, in supercooled melts, segregation of freshly formed nuclei by gravity would affect the final grain structure. Nonmetallic inclusions, gas bubbles and voids, which usually exist in melts, are also distributed nonuniformly by gravity.

Convection: In terrestrial processing, gravity is the primary driving force for the convection of contained fluids when they are subjected to thermal or concentration gradients. Temperature gradients arise from external heating and cooling, whereas concentration gradients are usually produced internally (Soret effect and solute rejection at freezing interfaces which leads

to "constitutional super-cooling"). These two gradients can produce density gradients large enough to induce buoyancy-driven flow. This fluid motion affects the temperature and concentration profiles within the fluid. This subsequently alters the shape and rate of movement of the freezing interface, because the kinetics of freezing depend on the local temperature and concentration. The degree of mixing caused by convection may be large enough to change the rate of solidification from kinetic to heat transfer or diffusion controlled which could drastically alter the grain structure. Examples of this convective effect on the transitions from planar to cellular or dendritic growth, from columnar to equiaxed eutectic structures, and from unidirectional to colonied or banded eutectic structures are cited frequently in the literature. Another effect of gravity-driven convection on solidification processes is that the bulk fluid movement, if rapid enough, can break delicate dendrite arms and thereby alter final grain structure. Furthermore, interlamellar spacing in eutectic growth and dendrite arm spacing are dependent on cooling rate which is a strong function of convection.

Hydrostatic Pressure: A body of fluid in a gravity field sustains a vertical pressure gradient as the bottom fluid must support the weight of the upper fluid. This pressure gradient distorts the shape of liquids on earth because the shape of a liquid surface is determined by the surface tension and the internal hydrostatic pressure (and adhesion if the liquid wets a solid surface). Distorted drops of liquid will result in nonsymmetrical solids upon freezing.

The following sections contain separate discussions for each experiment on the effects of microgravity on molten metal flow and solidification. For each experiment, the following topics are discussed: the most significant results to date; the expected low-g variations; and specific evaluations planned for Phase C. In the M551 Metals Melting Experiment, the relative magnitudes of convection in the molten pool and their effect on grain structure and shape have been analyzed. In the M552 Exothermic Brazing Experiment, the effects of gravity on capillary flow and capillary "gap" limits have been studied. In the M553 Sphere Forming Experiment, the magnitude of convection has been determined and how the grain structure, shape and surface finish of the spherical specimens should be affected.

Visual observation of flight and ground specimens, films (M551 and M553), and standard post-experiment metallurgical analyses will serve as the basis for comparing flight test data and specimens in the Phase C study. This will also empirically verify the Phase B study conclusions. These observations will consist of identifying convective stirring from film and identifying differences in structure, homogeneity, and/or unidirectionality in the post-experiment metallurgical analyses.

Section 2

M551 EXPERIMENT

The primary objective of this experiment is to study the melting and solidification of metals in reduced gravity. A second objective is to evaluate the electron beam (EB) process as a joining and cutting technique applicable to assembly and repair of structures in space. The primary goal of this particular study is to delineate the magnitude and pattern of the molten metal flow for both terrestrial and space flight processing conditions. From a knowledge of the convective differences and the other differences between terrestrial and space processing, the effects on grain structure and shape of the weld seam and dwell are to be predicted. The "other" differences of space versus ground processing include differences in sedimentation and beading (lack of hydrostatic pressure in space) and possible differences in vibration, radiation and vacuum levels. These last three effects are not predictable to a precise degree of accuracy and are no doubt negligible in comparison to microgravity and therefore will not be considered important. Also, it was shown in Phase A studies that terrestrial versus space flight convective differences were negligible in the continuous weld mode (Ref. 1). Thus the following discussions will concentrate on the dwell mode of the M551 experiment.

2.1 RESULTS

A summary of the most significant results found to date are given below:

- The following physical forces are operative during the cutting, joining and dwell portions of this experiment:

- Gravity/Acceleration
- Surface Tension
- Lorentz (beam current)
- Electrostriction
- Magnetostriction

Electrostatic Charges

Solidification Shrinkage

Thermal Expansion

Vaporization

EB Mechanical Pressure Force

- Significant molten metal motion was exhibited in each of the specimens filmed in both the dwell and weld (disk rotating) modes. The films examined thus far have all been ground tests.
- Both gravity and surface tension forces control molten metal flow during M551 ground tests. These natural convection driving forces arise because of severe nonisothermality during heating.
- Surface tension will still provide an equal magnitude of convection in zero-g, although the flow pattern may be different (see Appendix B).
- The mechanical pressure force associated with the impinging electron beam will not cause unstable splattering in the dwell mode, even in absolute zero gravity. Thus, any violent splattering can be attributed to surface tension or electro-magnetic instabilities at the weld pool surface or to degassing. This force is also negligible in comparison to surface tension, vaporization and/or hydrostatic forces during EB cutting.
- Sedimentation will not be a factor in this experiment, because vigorous stirring will occur both in terrestrial and Skylab operations.

The preceding conclusions were drawn from examination of color motion picture film taken during ground tests and from detailed examination of the descriptive differential equations which govern EB melting and solidification. The equations were examined using dimensional analysis (Refs. 2 and 3) and the nominal operating and boundary conditions for this experiment and the M512 chamber (Appendix A). Detailed derivations and results are given in Appendix B.

It should also be mentioned that surface tension, gravity and the electromagnetic forces are the most significant of all the preceding physical forces for convective motion. On Earth, gravity and surface tension are equal and dominant; whereas, on Skylab, surface tension will be dominant, followed by electromagnetic, then by gravity. Furthermore, there are two primary effects of surface tension on melt behavior:

- The mean effect of uniform surface tension results in normal stresses at free surfaces which determine the shape of fluids.
- Nonuniform surface tension leads to tangential stresses at free surfaces which can induce fluid motion.

2.2 EXPECTED LOW-G VARIATIONS

Based on the preceding results and conclusions, the following predictions are made regarding the variations expected in the disk welds processed in the microgravity conditions aboard Skylab:

- Slightly different grain structure and/or dendrite arm spacing may result due to different melt flow patterns (see Appendix B).
- Lack of hydrostatic pressure and dominance of surface tension will allow beading and dwell pool shape to be different (more spherical) and may cause deeper EB penetration.

The latter will occur because surface tension acts to pull the melt toward cooler surfaces which is away from the electron beam in this case. Assuming that the net gravitational field is always aligned with the beam in Skylab processing, the situations illustrated in Fig. 2-1 will result regarding bulk melt behavior of the dwell pool. As seen in Fig. 2-1a, surface tension dominance will pull the melt away from the beam, resulting in less resistance and deeper beam penetration than in terrestrial processing when heating from above. When heating from the side, however, terrestrial processing allows the melt to run out of the pool which will probably lead to even less resistance and more penetration than in space processing. Furthermore, the cut or seam may be asymmetric because of the uneven distribution of the melt in the terrestrial heating-from-the-side configuration.

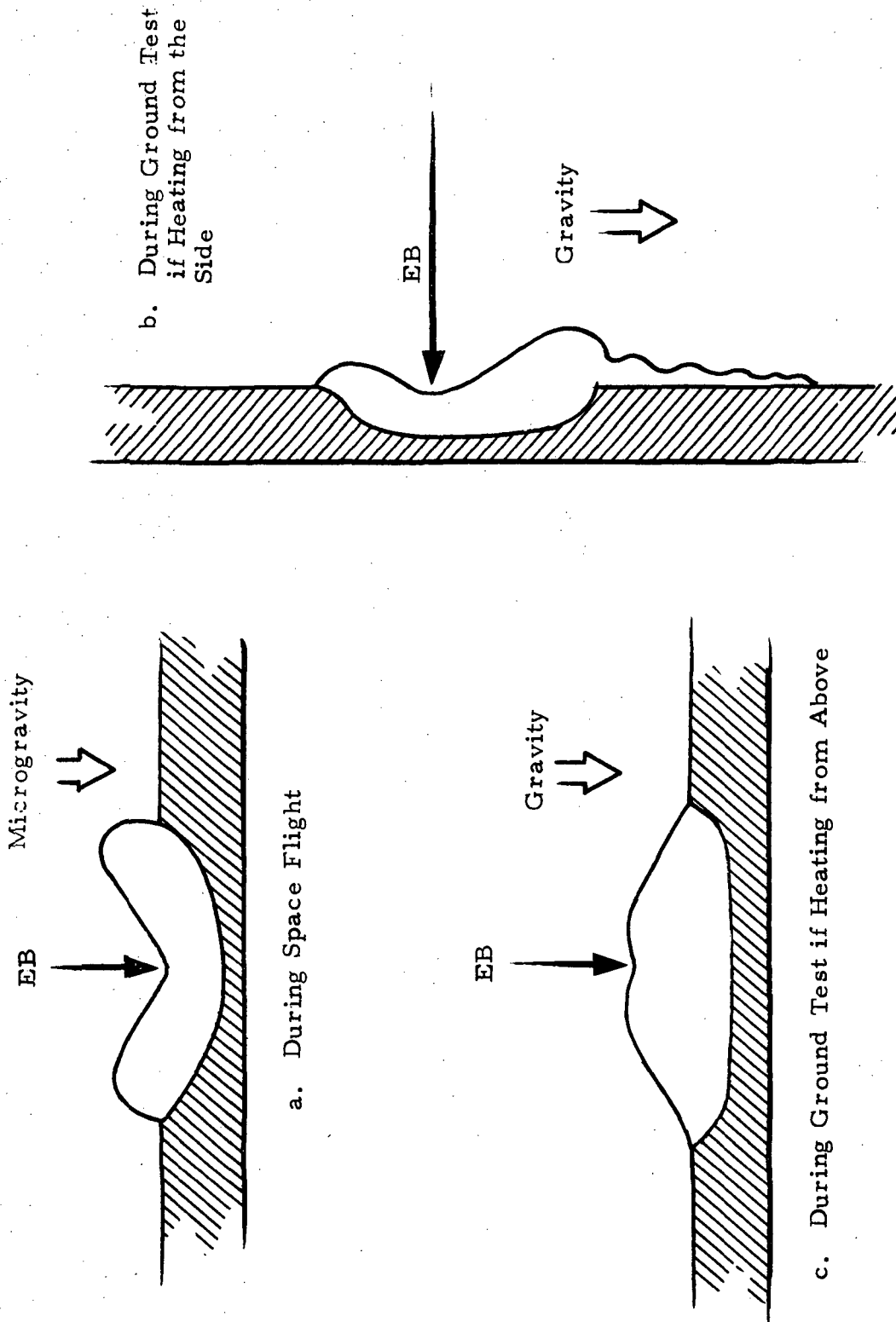


Fig. 2-1 - M551 Dwell Pool Behavior

2.3 PHASE C EVALUATIONS

Specific evaluations to be performed for this experiment in the Phase C portion of the study will include:

- The flight film will be examined and compared with ground test films to investigate differences in magnitude (velocity) of convection and flow patterns.
- The microstructure and grain size (to be obtained from other investigators) will be examined and compared with ground test results to observe if different melt shapes and convection patterns had any significant effects.

In addition, visual observations of flight and ground samples will be made to determine if beading and penetration changed significantly in space processing.

2.4 CONCLUSIONS AND SUMMARY

The primary conclusion of the preceding study is that significant stirring of the melt will occur both in terrestrial and space processing for the M551 experiment. The magnitude of this convective fluid flow will be the same in both environments. The flow patterns, however, will be different because surface tension alone will be the convective driving force for Skylab processing whereas gravity and surface tension forces will be equally coupled driving forces on Earth. As a result of surface tension dominating pool shape, quicker, cleaner, narrower and more symmetrical cuts and penetrations should be attainable in EB melting in space.

It is recommended that the M551 experiment be repeated in the space environment essentially as is except that high-speed photography should be added. This will allow important hydrodynamic phenomena in cutting, beading, and the dwell to be studied. The current 24 ft/sec filming rate of the flight test will miss much of the hydrodynamic behavior of the melt. An accurate description of the hydrodynamics involved may settle debates which currently exist over how the beam penetrates and what causes rippling. Further recommendations include the following additions to M551 experiment objectives:

- Study surface tension dominated fluid flow in the absence of gravity. In terrestrial studies, gravity forces usually predominate and cloud all other effects.
- Study the fluid dynamics involved in EB melting. Understanding of the stirring and heat flow associated with convective motions should be a valuable contribution to EB welding regardless of whether terrestrial or space applications are being considered.

Section 3

M552 EXPERIMENT

The primary objectives of this experiment are to study and evaluate the capillary flow of molten braze material, to evaluate a tube joining technique for the assembly and repair of hardware in space, and to demonstrate the feasibility of exothermic reaction in space. The primary goal of this particular study is to predict the effects of gravity on capillary flow and capillary "gap" limits. Accounting for these differences in capillary flow and other space-versus-Earth processing differences (e.g., sedimentation, lack of hydrostatic pressure, vacuum, etc.), changes in braze solidification are to be estimated.

3.1 RESULTS

A summary of the most significant results found to date are:

- Spreading time will be up to 50% shorter in gravity fields anticipated for Skylab than in ground tests.
- Turbulent or oscillatory laminar flow will occur for some gap widths in M552 Skylab processing, whereas only steady laminar flow would occur on Earth.
- Marangoni bubble migration will probably be important for M552 Skylab conditions, whereas buoyancy will control bubble location under terrestrial conditions. The Marangoni effect is a surface tension force which can drive fluid motion. It can arise from temperature or concentration gradients. In the present case, only temperature gradients are considered.
- The extent of capillary rise or spreading will be increased in zero gravity. This will be an especially significant result in cases where the capillary driving pressure has the hydrostatic pressure of the liquid column opposing it during terrestrial operations.
- The density ratio of silver to copper is $\rho_{Ag}/\rho_{Cu} = 1.2$, which means that silver may have a tendency to settle to the bottom of the joint on Earth, but would remain mixed on Skylab.

The detailed calculations and data upon which the preceding results were derived are given in Appendix C.

It is very important that the spreading time and fluid flow conditions be known in brazing. At first glance the flow analysis suggests that the time required to fill the joint is insignificant compared with the overall time of the brazing operation. This is not the case, however, when one considers rapidly occurring interactions such as alloying between the base and filler metal, differential rates of vaporization between the braze alloy constituents, and electrocapillarity (layers of ions alter the surface free energy of the filler).

These and other detrimental interactions, along with the importance of a knowledge of fluid flow conditions, are explored in detail by Milner (Ref. 4). Many of the important interactions with capillary flow in brazing operations are due to the presence of the fluxing agent. Fluxes remove the initial oxide film but may not entirely prevent further reoxidations. The use of a flux may also modify wetting and filling of a joint by:

- Electrochemical reactions between the base and filler metal with the flux acting as an electrolyte.
- Electrocapillarity in which layers of ions change the surface free energy.
- Substitutional chemical reactions in which an element of the flux is deposited on the surface of the base metal.

Alloying between the braze and base metal can radically affect joint filling by changing the surface tension, viscosity and melting point of the filler metal. Surface roughness can have an important effect as it may reduce a contact angle of up to 80 degrees down to zero. Surface roughness is also related by some to the well-known dynamic capillary effect known as contact angle hysteresis (Refs. 5 and 6). The quicker the molten braze spreads, the less time there will be for the preceding interactions to significantly alter spreading.

3.2 EXPECTED LOW-G VARIATIONS

Using the preceding results and conclusions as a foundation, the following predictions can be made regarding the variations expected in the brazed joints processed in the microgravity environment aboard Skylab:

- The extent, rate and uniformity of spreading should be increased in low gravity which should lead to better joints. If turbulence occurs in wider gaps, this improvement may not be attained.
- The lack of hydrostatic pressure should allow a more symmetrical interface at the free surface of the filler and permit capillary spreading in wider gaps.
- The location of bubbles or voids should be different between Earth and Skylab processing and will depend on container orientation to gravity direction and the magnitude of effective gravity during the brazing operation.

The first item above is based on the premise that faster, laminar flow rates will allow less time for deleterious interactions to occur in the spreading molten braze.

The last two variations are directly dependent on the exact magnitude and direction of the gravity vector which will be operating during Skylab processing of M552. The magnitude of gravity aboard Skylab during the M552 experiment will be approximately $10^{-5} g_E$ ($g_E = 9.8 \text{ m/sec}$), but the gravity direction is not yet known. Thus, precise predictions on bubble or void location cannot be given at the present time.

3.3 PHASE C EVALUATIONS

Specific evaluations to be performed for this experiment in the Phase C portion of the study will include:

- The extent and uniformity of spreading will be examined using data supplied by other investigators.
- The location of voids will be evaluated taking into account solidification shrinkage, buoyancy, Marangoni effect and the presence of the tube slot.

- The microstructure data obtained by others will be analyzed, especially near the free surface where surface tension convection might occur even in low gravity.

In addition, visual observations of sectioned flight and ground samples may provide direct information of the extent of spreading and voidage changes which occurred in space processing.

3.4 CONCLUSIONS AND SUMMARY

The primary conclusion to be drawn from the preceding discussions is that better quality joints may result due to the increased extent, rate and uniformity of spreading attainable in the microgravity environment aboard Skylab. If turbulence occurs in the wide gap specimens, this improvement may not be seen for these specimens. Also, based on the aforementioned results and conclusions, a new experiment involving the brazing of extra-wide gaps and several new configurations of variable size gaps (e.g., eccentric annuli at acute angles of departure) is suggested.

Section 4

M553 EXPERIMENT

The basic objective of this experiment is to determine the effects of reduced gravity on fundamental solidification phenomena. In particular, the following two effects should be prominent:

- The density difference between components (e.g., nickel and tin) will not lead to sedimentation as might occur in terrestrial operation.
- The specimens may be cast from the melt without using containers or molds (homogeneous nucleation).

The primary goal of this particular study is to delineate the magnitude and pattern of the molten metal flow for both terrestrial and space flight processing conditions. From a knowledge of the convective flow differences and the other differences between terrestrial and space processing, solidification theory will be utilized to predict how the grain structure, shape, internal voidage and surface finish of the spherical specimens should be affected. The "other" differences of space versus ground processing include changes in sedimentation and sphericity (lack of hydrostatic pressure and dominance of capillary forces in space) and possible differences in vibration, radiation, electromagnetic, and vacuum levels. The last four effects are not predictable to a precise degree of accuracy and are no doubt negligible in comparison to microgravity effects and will therefore not be considered important.

4.1 RESULTS

A summary of the most significant results found to date are given below.

- The following physical forces are operative on the M553 specimens during EB melting and solidification:
 - Gravity/Acceleration
 - Surface Tension
 - Lorentz (beam current)
 - Electrostriction
 - Magnetostriction
 - Electrostatic Charges
 - Solidification Shrinkage
 - Thermal Expansion
 - Vaporization
 - EB Mechanical Pressure Force
- Vigorous convective stirring occurs in the molten metal for each of the M553 sample materials. This fluid motion was exhibited on high speed motion picture film taken for both ground tests and low gravity KC-135 aircraft tests.
- Both gravity and surface tension forces control molten metal flow during M553 ground tests. These natural convection driving forces arise because of severe non-isothermality during heating.
- Surface tension driven convection will occur in Skylab electron beam melting. In the near absence of gravity, the surface tension forces will provide an equivalent amount of convection aboard Skylab, but the flow pattern may be different from those of operations on Earth.
- Velocities of 20 cm/sec magnitude will be attained 0.1 sec after melting begins in the M553 nickel specimen (both for Skylab and ground tests). Fluid flow will decay 60 seconds after melting begins. This means that some degree of flow will exist upon freezing even for the free-floating M553 spheres.

- The mechanical pressure force associated with the impinging electron beam is not the cause of violent droplet breakup exhibited in some of the earlier KC-135 aircraft tests. Thus, any unstable splattering of the melt during heatup must be attributed to surface tension or electromagnetic instabilities at the melt surface or to degassing.
- Sedimentation will not be a factor in this experiment, because vigorous stirring will occur both in terrestrial and Skylab operations.

The preceding conclusions were drawn from examination of color motion picture film taken during ground and low-gravity aircraft flight tests and from detailed examination of the descriptive differential equations which govern EB melting and solidification. The equations were examined using dimensional analysis (Refs. 2 and 3) and the nominal operating and boundary conditions for this experiment and the M512 chamber (Appendix A). Detailed derivations and results are given in Appendix D.

It should also be mentioned that surface tension, gravity and the electromagnetic forces are the most significant of all the preceding physical forces for convection. On Earth, gravity and surface tension are equal and dominant; whereas, on Skylab, surface tension will be dominant, followed by electromagnetic, then by gravity. Furthermore, there are two primary effects of surface tension on melt behavior:

- The mean effect of uniform surface tension results in normal stresses at free surfaces which determines the shape of fluids.
- Nonuniform surface tension leads to tangential stresses at free surfaces which can induce fluid motion.

4.2 EXPECTED LOW-G VARIATIONS

Based on the previous results and conclusions, the following predictions can be made regarding the variations expected in the specimens processed in the microgravity environment of Skylab:

- The primary differences expected in Skylab samples will be due to containerless casting; i.e., there will be no wall effects upon nucleation and solidification. Thus dendritic and grain structure should be finer because of the large degree of supercooling which can be obtained in homogeneous nucleation. Containerless, free suspension will also provide more perfectly spherical castings.
- Solidification shrinkage may induce imperfections in the sphericity of the castings. Furthermore, shrinkage may cause a number of voids or one large shrinkage cavity in the interior of each casting. The latter may occur symmetrically and form the basis for "hollow ball bearings."
- Finally, the residual fluid motion existing at the instant of freezing may introduce some inhomogeneity in the microstructure.

4.3 PHASE C EVALUATIONS

Specific evaluations to be performed for this experiment in the Phase C portion of the study are given below.

- The flight film will be examined and compared with KC-135 aircraft and ground test films to investigate differences in magnitude (velocity) of convection and flow patterns.
- The microstructure and grain size (to be obtained from other investigators) will be examined for evidences of convective effects.

In addition, visual observations of flight and ground specimens will be performed to determine if sphericity and surface finish improved markedly in space processing.

4.4 CONCLUSIONS AND SUMMARY

The primary conclusion of the preceding discussions is that significant flow and stirring in the molten spheres (during and after EB melting) will occur in both terrestrial and space processing. The magnitude of this convective fluid motion

will be the same in both environments. The flow patterns, however, will be different because surface tension alone will be the convective driving force for Skylab processing whereas gravity and surface tension forces will be equally coupled driving forces on Earth. As a result of surface tension dominating specimen shape, more perfectly spherical and smoother spheroids should be obtainable. This experiment may also engender the production of thick-walled hollow spheres which would have ready application as hollow ball bearings. Furthermore, the unique microstructures attainable through containerless nucleation and solidification may yield castings with unusual structural (strength) or electromagnetic properties.

It should be noted that a repeat of this experiment in the microgravity environment of space as is, except for longer, higher speed camera coverage, would yield much more hydrodynamic information. This information is important because hydrodynamics controls the release of the specimens and affects the solidification and microstructural properties. The release mechanism is of utmost importance because it will control the duration of free float time in the absence of acoustic or electromagnetic levitation. It is recommended that a new experiment be performed with no active mechanical forces (springs) for release, i.e., allow only the vaporization and electromagnetic forces to initiate release. The slight forces could be counteracted by the small residual gravity field to yield very slow release acceleration and extremely long free-float times.

Further recommendations include the following additions to M553 experiment objectives.

- Study surface tension driven convection (due to non-uniform temperature) in free floating, molten spheroids. Similar types of fluid flow probably exist in stars such as the Sun, and this information should be of great interest to astronomers.
- Study the hydrodynamics and kinematics of deployment in zero-g. This step is critical for obtaining long periods of free float which will be essential to future space processing applications.

- Study the fluid dynamics involved in electron beam melting. Understanding of the stirring and heat flow associated with convective motions should be a valuable contribution to EB melting and solidification regardless of whether terrestrial or space applications are being considered.

REFERENCES

1. Bourgeois, S. V., and P. G. Grodzka, "Convection in Space Processing - Phase A Report," LMSC-HREC D306065, Lockheed Missiles & Space Company, Huntsville, Ala., July 1972.
2. Churchill, S. W., and J. D. Hellums, "Dimensional Analysis and Natural Convection," Chem. Engr. Prog. Symp. Ser. (Heat Transfer-Buffalo), Vol. 57, 1964, p. 75.
3. Ostrach, S., "Role of Analysis in the Solution of Complex Physical Problems," Third Intl. Heat Trans. Conf., Chicago, August 1966.
4. Milner, D. R., "A Survey of the Scientific Principles Related to Wetting and Spreading," Brit. Weld. J., March 1958, pp. 90-105.
5. Blake, T. D., and J. M. Haynes, "Contact Angle Hysterisis," Progress in Surface and Membrane Science, Vol. 6, 1973, pp. 125-138.
6. Rose, W., and R. W. Heins, "Moving Interfaces and Contact Angle Rate Dependency," J. Colloid Sci., Vol. 17, 1962, pp. 39-48.

Appendix A

**NOMINAL OPERATING CONDITIONS
FOR THE SKYLAB M512 CHAMBER**

Appendix A

In this appendix a compilation is presented of pertinent environmental conditions for the M512 experiments to be performed aboard the first Skylab mission. Also included is a summary of convection sensitivity calculations for the M512 experiments.

The M512 facility will contain several experiments (M551, M552, M553, M566) for the investigation of melting and solidification in a space environment. Convection in the molten fluid may be a controlling parameter in these processes. In order to evaluate convection and other phenomena, the pertinent environmental conditions of each experiment must be known. This appendix contains a compilation of the factors that are important for assessing convection.

The environmental conditions expected for each experiment are shown in Table A-1. Data enclosed within parentheses indicate that they are estimates and need further study. Also some categories have no data which indicates that these factors could not be estimated at the present time.

Dimensionless ratios which give an indication of convection sensitivity for each M512 experiment are shown in Table A-2. These numbers were evaluated by estimating pertinent temperature gradients from documented ground-base studies, Brown Engineering thermal analyzer studies and Lockheed thermal studies and utilizing the data in Ref. A-1. The table contains Rayleigh numbers (Ra), Marangoni numbers (Ma), thermal diffusivities (α), Prandtl numbers (Pr), and Stefan numbers (St) which have been obtained for the molten metals in the M551, M552, M553 and M566 experiments. Critical Rayleigh (Ra_c) and Marangoni (Ma_c) numbers for these experiments were estimated from the literature (Refs. A-2, A-3, and A-4). When the Rayleigh number exceeds its critical value, gravity-induced convection will occur and

Table A-1
ENVIRONMENTAL CONDITIONS FOR M512

Condition	M551	M552	M553	M554
Date/Time of Experiment		5/8/73		
Gravity Level (cm/sec ²)		(.001 - .1)		
Gravity Gradient (1/sec ²)				
Initial Chamber Pres. (atm)	←	(0.34)	→	
Initial Atmos. Composition in Chamber (wt %)		(O ₂ (70), N ₂ (30))		
Initial Chamber Temp. (°C)		(10 - 32)		
Electron Beam				
• Wattage	1.6 kW		(1.2 kW)	
• Amperage	80 mA		50-60 mA	
• Focus	.03 - .09 in.		.25 in.	
• Duration	15 - 30 sec		3-5 sec/sphere	
• X-ray level	(> 20 μrad/sec)		(>20 μrad/sec)	
Magnetic Field Level				
Vibration Levels				
• Amplitude (cm)				
• Frequency (Hz)				
Electrical Fluctuations				
Wheel Rotation				
• Rate (rpm)	2.5 ± 0.1			
• Radius (cm)	8.25			
• Weld Radius (cm)	6.04			
Cabin Conditions				
• Temperature (°C)		20 - 25		
• Pressure (atm)		0.34		
• Composition (wt %)	←	O ₂ (70), N ₂ (30)	→	
Space Atmosphere				
• Temperature (°C)		950 - 1160		
• Pressure (torr)		10 ⁻⁶ - 10 ⁻⁸		
• Composition	10 ⁶ e/cc, 10 ⁸ neut.	particles/cc, MW = 20-26		
Chamber Size				
• Volume:	←	1.5 cu ft	→	
• Diameter:		16.25 in.		
Size of Valve to Space:		4 in. vent valve (40 in. long tube to space)		

Table A-2
SENSITIVITY ANALYSIS OF M512 EXPERIMENTS

Material	Ra _c	Ra (10 ⁻⁴ g)	Ra (lg)	Ma _c	Ma	α (cm ² /sec)	Pr	St
2219 Aluminum (Continuous Weld)	1500	10 ⁻⁴	1.0	80	1.3	0.325	0.015	2 x 10 ⁻⁴
321 SS (Dwell)	1500	5.7	57,400	80	236,000	0.165	0.046	4 x 10 ⁻²
Tantalum	1500	—	—	80	—	0.155	0.013	4 x 10 ⁻²
Braze Alloy	1700	10 ⁻²	62	—	800	0.202	0.021	—
Nickel	700	.24	2,370	200	12,900	0.120	0.054	2 x 10 ⁻³
Ni-Sn	700	.21	2,130	200	5,530	0.130	0.043	2 x 10 ⁻³
Ni-Cu	700	.15	1,480	200	5,750	0.125	0.048	4 x 10 ⁻³
Al-Cu Eutectic	90	.19	1,900	—	7,000	0.284	0.019	—

significantly affect heat transfer. Similarly, if the critical Marangoni number is exceeded, surface tension-driven convection will occur. The Stefan number is useful in analyzing radiative cooling (M551 and M553) and the thermal diffusivity and Prandtl number are useful in studying thermal profiles and fluid motion. Table A-3 represents a quick comparison of the modes of convection expected in M512 experiments on Earth and on Skylab.

It must be emphasized that the critical conditions only rigorously apply when gravity is aligned with and opposed to the temperature gradient. It is also assumed that uniform heating exists (linear temperature gradient) and that temperature gradients only occur in one direction. With these restrictions in mind, the conclusions in Table A-3 give an accurate indication of the convection modes which should be expected for these experiments.

No values for Ra and Ma are shown for tantalum because a reliable estimate of tantalum's thermal conductivity in the molten state has not yet been found. Similarly the critical Marangoni numbers for M566 and M552 are not given because Ma_c has not been estimated in the literature for such large aspect ratio configurations. Values of the Stefan number for these two experiments are not given because melt radiation will not be a factor.

The Rayleigh number, Ra, is the weighted ratio of the buoyancy driving force to the viscous forces which tend to resist fluid flow and is defined by,

$$Ra = \frac{gd^3\beta\Delta T}{\nu\alpha}$$

where g is the gravity acceleration, d the depth of the fluid layer, β the thermal volumetric expansion, ΔT a temperature difference in the fluid, ν the kinematic viscosity, and α the thermal diffusivity. A corresponding number of surface tension force to viscous force is given by the Marangoni number:

Table A-3

GRAVITY AND SURFACE TENSION CONVECTION IN M512 EXPERIMENTS

Experiment	Material	Gravity-Driven		Surface Tension-Driven
		1g	10^{-4} g	
M551	2219 Al (Rotating Disk)	No	No	No
	321 SS (Dwell)	Yes	No	Yes
M552	Ag-Cu Braze Alloy	No	No	No
M553	Nickel	Yes	No	Yes
M554	Al-Cu	Yes	No	No

Appendix B

DETAILED ANALYSES FOR THE
M551 EXPERIMENT

Appendix B

This appendix contains detailed results of calculations for the M553 experiment which were performed during the Phase B portion of this study. The first section contains an analysis of the driving forces, magnitude and pattern of natural convective fluid flows which occur in the Sphere Forming Experiment. This section is followed by a discourse on the possibility of molten pool splattering due to the momentum of the impinging electron beam.

B.1 CONVECTION ANALYSIS

B.1.1 Summary

Results to date of the convection analysis indicate that: (1) surface tension is the main driving force for fluid motion in microgravity electron beam welding; (2) gravity forces also predominate in ground-based welding; (3) vapor pressure is the primary cause of surface deflection (cutting action); (4) high-speed photography (2000 frames per second) of KC-135 or ground-based tests are required; and (5) fluid dynamics undoubtedly control the mixing, microstructure, and shape of the weld pool in the electron beam weldings.

B.1.2 Dimensional Analysis

As in the other M512 experiments, the fluid dynamics of the M551 experiment is the most important factor in determining quality of the final product (in this case, the solidified pool, seam and cut produced on various areas of thin metal disks). Flow patterns in the molten material are important in these experiments, because all of the materials have low entropies of fusion (Ref. B-1). Thus, their solidification (microstructure) is controlled by the rate of heat transfer removal (Ref. B-2), which changes with the fluid flow

(Refs. B-3 and B-4). The flow will be especially important in the dwell mode, since a relatively large pool of melt will be created. The degree of flow will also determine the amount of mixing attained. If no or little flow were present, all heavier components would segregate to the bottom of weld zones on earth, but to a much lesser extent in microgravity environments. Fluid flow can also affect the shape of the weld pool (Ref. B-7).

Application of dimensional analysis (Refs. B-5 and B-6) to the governing equations for EB welding, coupled with ground-based and KC-135 experiments, should enable prediction of the extent of reduction or increase of motion in the weld pool and/or the change in flow pattern in electron beam welding in space. Possible physical forces which could induce fluid flow in the M551 experiment, and their causes, include:

- Effective Gravity Force: Resultant force on weld specimen due to earth's gravity and centrifugal and coriolis forces of orbiting spacecraft.
- Lorentz Force: Electromagnetic forces induced by passage of the electron beam current through the specimen.
- Electrostriction: Stresses induced when electrical permittivity changes with density.
- Magnetostriction: Stresses induced when permeability changes with density.
- Electrostatic Force: Caused by presence of excess electrical charge (due to beam current and/or thermionic emission).
- Surface Tension: Tangential stresses at vapor-liquid or liquid-liquid interfaces can be induced if surface tension depends on temperature and/or concentration. Surface tension will also cause pressure gradients across curved interfaces.
- Density Differences Accompanying Phase Changes
- Beam Force: Impinging electrons give up their momentum.

- Thermal Expansion: Dilation and compression of fluids whose density changes appreciably with temperature can induce fluid flow.
- Vibration: Uncontrolled movement due to engine operation, astronaut motion, particle impacts, etc.
- Centrifugal and Coriolis: Generated by disk rotation.
- Vapor Pressure: Evaporating molecules impact momentum which leads to normal stresses at vapor-liquid interface.
- Inertia Forces: Tend to sustain induced motions.
- Viscous Forces: Tend to resist driving forces.

The preceding forces, which could influence fluid flow and solidification, appear explicitly in the conservation equations which apply to formation of a molten pool by electron beam heating. These equations are given in detail in Appendix D.

A formal method of determining the controlling physical forces affecting fluid flow and solidification in electron beam welding was introduced in Appendix D, Section D.1.2. The controlling physical forces are determined by non-dimensioning the governing differential equations and performing an order-of-magnitude comparison on the various dimensionless groups which result. The key to successful analysis is in choosing the proper reference values; i.e., since no freestream velocity exists, which forces do we equate to estimate a "characteristics" or "typical" velocity. Choosing the proper characteristic velocity is very important, since the reference time, temperature, etc., usually depend on this velocity. The results arrived at in Appendix D, Section D.1.2 are also valid for the M551 experiment.

The equation, in dimensionless form, governing electron beam melting is Eq. D-1 shown in Appendix D. Values of the pertinent dimensionless groups for each of the M551 materials are given in Table B-1. Examining Table B-1

Table B-1
M551 DIMENSIONAL ANALYSIS

Material	N_{Oh}	N_{Bo}	$\frac{1}{N_{Oh}}$	$\frac{N_{Bo}^*}{N_{Oh}}$	$\frac{N_{Bo}^\dagger}{N_{Oh}}$
2219 Aluminum	5.8×10^{-4}	3.09	1713	5287	0.53
321 Stainless Steel	6.3×10^{-4}	1.56	1581	2461	0.25
Tantalum	3.4×10^{-4}	7.19	2942	21150	2.11

* With Earth gravity (9.8 m/sec^2)

† With 10^{-4} Earth gravity

in conjunction with Eq. (D.1), an order-of-magnitude analysis indicates that surface tension driven convection will occur both in ground tests and for Skylab conditions because $N_{Oh} \ll 1$. Furthermore, gravity driven convection will exist on ground tests, but will be negligible in the reduced gravity of Skylab. Thus different forces will control convection on earth versus Skylab. The preceding analysis also indicates that electromagnetic or Lorentz forces will be negligible with regard to causing fluid motion. See Appendix D, Section D.1.2 for further details.

A review of the literature on electric arc welding, which is somewhat similar to electron beam welding, has generated the following facts which can be compared to the preceding conclusions. In a study of motion in weld pools in arc welding, Woods and Milner (Ref. B-7) conclude that Lorentz forces are the primary cause of motion. An additional secondary cause is the momentum imparted by the impinging arc. Surface tension forces were not considered. Kotecki et al. (Ref. B-8) showed that surface tension and momentum forces of the impinging arc controlled ripple formation in gas tungsten arc welds. Surface tension controls when the arc is shut off. Brimacombe and Weinberg (Ref. B-9) also conclude that surface tension is the driving force for fluid motion once the impinging jet is removed.

One direct result of formulating the governing equations is that surface deflection (cutting action) is primarily caused by vapor pressure, but that the beam force is also appreciable. This was determined from the vapor-liquid force equation of Section D.1.2, which indicates that,

$$\frac{\text{Vapor Pressure}}{\text{Beam Pressure}} \approx 2$$

This agrees with earlier studies (Ref. B-10).

B.1.3 Flow Patterns

The aforementioned difference in controlling forces between terrestrial and space processing for the M551 experiment should result in altered flow patterns between these two conditions. From a knowledge of flow patterns generated by surface tension versus buoyancy controlled convection on Earth (Ref. B-11), the situation illustrated in Fig. B-1 would no doubt exist during melting on Earth, while that shown in Fig. B-2 would prevail in space. These two figures represent cross-sectional views through the molten dwell pool. The pattern shown in Fig. B-2 is based on the fact that surface tension is stronger in cooler regions; therefore the coolest portion of the specimen will exert the strongest "pull" on the surface. In both cases, the motion is termed cellular (Ref. B-11).

These predicted flow patterns have been verified by M551 ground tests. Movies taken during ground-based tests of the M551 experiment for all three materials (2219 aluminum, stainless steel and tantalum) were studied during the week of 16 March 1973. The quality of the film and the resolution of the fluid flow in the weld pool were excellent in several of the tests. Four distinct Benard convection cells were observed in the weld pool of a stainless steel dwell. Significant molten metal motion was exhibited in each of the specimens filmed in both the dwell and weld (disk rotating) modes.

3.2 WELD POOL SPLATTERING

In both the M551 and M553 experiments, the heat released to the metal specimens by the impinging electron beam enables a molten pool to form. A question arises as to the stability of these molten liquids in low gravity. At least one of the KC-135 M553 specimens was seen to break up violently into many smaller liquid spheroids upon complete melting. The electron beam was still hitting the specimen during break up. A similar instability might develop in the molten puddle formed during the dwell mode of the M551 experiment, wherein the liquid might not adhere and separate from the solid disk (violent splattering).

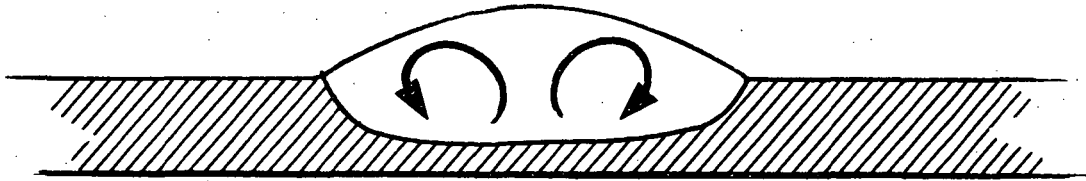


Fig. B-1 - Convective Pattern in M551 Dwell Pool
Melting on Earth



Fig. B-2 - Convective Pattern in M551 Dwell Pool
During Melting in Space

There are at least three different mechanisms which might explain the instability observed in the M553 KC-135 specimens. Upon melting, the specimen may have experienced violent degassing which could have led to droplet breakup. Another mechanism might be electrohydrodynamic instability caused by interactions between the electromagnetic forces of the electron beam and the fluid flow field set up in the molten metal by both thermal gradients, Lorentz and other forces (Ref. B-12). Lastly, the momentum force associated with the impinging electron beam might have set up unstable surface oscillations on the molten metal.

The latter instability mechanism has been treated recently by Berghmans (Ref. B-13). He performed a theoretical study of fluid interface stability with special attention being given to the role of surface tension. It was motivated by its possible application to the splattering of molten metal as observed during electric arc welding.

Berghmans' study concluded that the weld pool interface would be stable if the following condition was met,

$$We^2 \leq 1.04 + 3.3 Bo^2 \quad (B.1)$$

where

We = Weber number

Bo = Bond number

The analysis is only rigorous if inertia and viscous effects are small compared to surface tension effects. Inertia effects are not negligible in the M551 and M553 experiments, but the results of Berghmans' study should give a reasonable approximation.

The criterion expressed by Eq. (B.1) were applied to each of the materials in both the M551 (2219 aluminum, stainless steel, and tantalum) and the M553

(pure nickel, Ni-Cu, Ni-Ag, and Ni-Sn) and for gravity levels between ground tests ($g_E = 980 \text{ cm/sec}^2$) and those of Skylab ($g = 10^{-5} g_E$). Beam diameter was also varied between 0.635 and 0.07 cm. For each of the above cases,

$$We^2 < 10^{-2}$$

therefore, the momentum force of the electron beam will not be a primary cause of weld pool instability in either M551 or M553.

REFERENCES

- B-1. Laudise, R.A., J.R. Carruthers, and K.A. Jackson, "Crystal Growth," in Annual Review of Materials Science, Vol. 1, 1971, pp.253-256.
- B-2. Laudise, R.A., The Growth of Single Crystals, Prentice, Hall, Englewood Cliffs, N.J., 1970, pp. 86-103.
- B-3. Goldak, J.A., G. Burbidge and M.J. Bibby, "Predicting Microstructure from Heat Flow Calculations in Electron Beam Welded Eutectoid Steels," Can. Met. Quart., Vol. 9, 1970, p.459.
- B-4. Ibid, p.467.
- B-5. Churchill, S.W., and J.D. Hellums, "Dimensional Analysis and Natural Convection," Chem. Engr. Prog. Symp. Ser., Vol.57, 1964, p.75.
- B-6. Ostrach, S., "Role of Analysis in the Solution of Complex Problems," Third Intl. Heat Trans. Conf., Chicago, August 1966.
- B-7. Woods, R.A., and D.R. Milner, "Motion in the Weld Pool in Arc Welding," Welding J., p.163s, April 1971.
- B-8. Kotecki, D.J., D.L. Cheever and D.G. Howden, "Mechanism of Ripple Formation During Weld Solidification," Welding J., p.386s, August 1972.
- B-9. Brimacombe, J.K., and F. Weinberg, "Surface Moments of Liquid Copper and Tin," Met. Trans., Vol.3, p.2298 (1972).
- B-10. Wells, O.C., and T.E. Everhardt, "A Note on the Physical Principles Underlying the Formation of the Cavity in Electron Beam Welding," Proc. 4th Symp. Elec. Beam Tech., Boston, 1962, p.106.
- B-11. Grodzka, P.G., "Types of Natural Convection in Space Manufacturing Processes," LMSC-HREC TR D306350, Lockheed Missiles & Space Company, Huntsville, Ala., December 1972.
- B-12. Torza, S., R.G. Cox and S.G. Mason, "Electrohydrodynamic Deformation and Burst of Liquid Drops," Phil. Trans. Roy. Soc. London, Ser. A, Vol. 269, 1971, p.295.
- B-13. Berghmans, J., "Theoretical Investigation of the Interfacial Stability of Inviscid Fluids in Motion, Considering Surface Tension," J. Fluid Mech., Vol. 54, 1972, pp. 129-141.

Appendix C

DETAILED ANALYSES FOR THE
M552 EXPERIMENT

Appendix C

This appendix contains detailed results of calculations for the M552 experiment which were performed during the Phase B period of this study. The first portion of the appendix addresses the capillary flow analysis, while the second segment discusses bubble dynamics associated with M552.

C.1 M552 CAPILLARY FLOW

The effect of gap width and low gravity on capillary flow in the M552 Exothermic Brazing Experiment has been studied. Time-to-spread, flow velocities and Reynolds number have been calculated for the configuration shown in Fig. C-1. The results are shown in Tables C-1, C-2 and C-3.

The results indicate that:

- Spreading time will be up to 50% shorter in gravity fields anticipated for Skylab than in ground tests.
- Turbulent or oscillatory laminar flow will occur in Skylab processing in certain gaps where only laminar flow could occur in ground tests.

The flow equation for an annulus is given by,

$$u = \frac{\rho g R^2 \phi}{8 \mu h} (h_o - h) \quad (C.1)$$

where

- u = velocity
- h = axial position in annulus
- ρ = density
- R = sleeve radius
- μ = viscosity
- k = tube radius/sleeve radius

Table C-1
M552 SPREADING TIMES

Gravity (g/g _E)	Gap Width (in.)	Spread Time (Annulus) (μ sec)
$2 \cdot 10^{-6}$.005	12.00
	.010	6.00
	.020	2.97
	.030*	1.76
1	.005	13.60
	.010	7.47
	.020	4.42
	.030*	3.60

* Assuming no variation in gap width.

Table C-2
M552 FLOW VELOCITIES

Geometry	Gravity (g/g _E)	Gap (in.)	Velocity (u) (cm/sec)
Annulus	$2 \cdot 10^{-6}$.005	34
		.010	67
		.020	134
		.030*	200
	1	.005	30
		.010	55
		.020	90
		.030*	97
Slot	$2 \cdot 10^{-6}$.005	33
		.010	66
		.020	132
		.030*	198
	1	.005	30
		.010	53
		.020	81
		.030*	84

* Assuming no variation in gap width.

Table C-3
M552 REYNOLDS NUMBERS

Geometry	Gravity (g/g _E)	Gap (in.)	Re ₁	Flow Regime
Annulus	2·10 ⁻⁶	.005	202	Laminar
		.010	794	Oscillatory
		.020	3200	Turbulent
		.030*	7210	Turbulent
	1	.005	182	Laminar
		.010	650	Laminar
		.020	2170	Oscillatory
		.030*	3490	Turbulent
Slot	2·10 ⁻⁶	.005	99	Laminar
		.010	395	Laminar
		.020	1580	Laminar
		.030*	3550	Turbulent
	1	.005	90	Laminar
		.010	315	Laminar
		.020	970	Laminar
		.030*	1500	Laminar

* Assuming no variation in gap width.

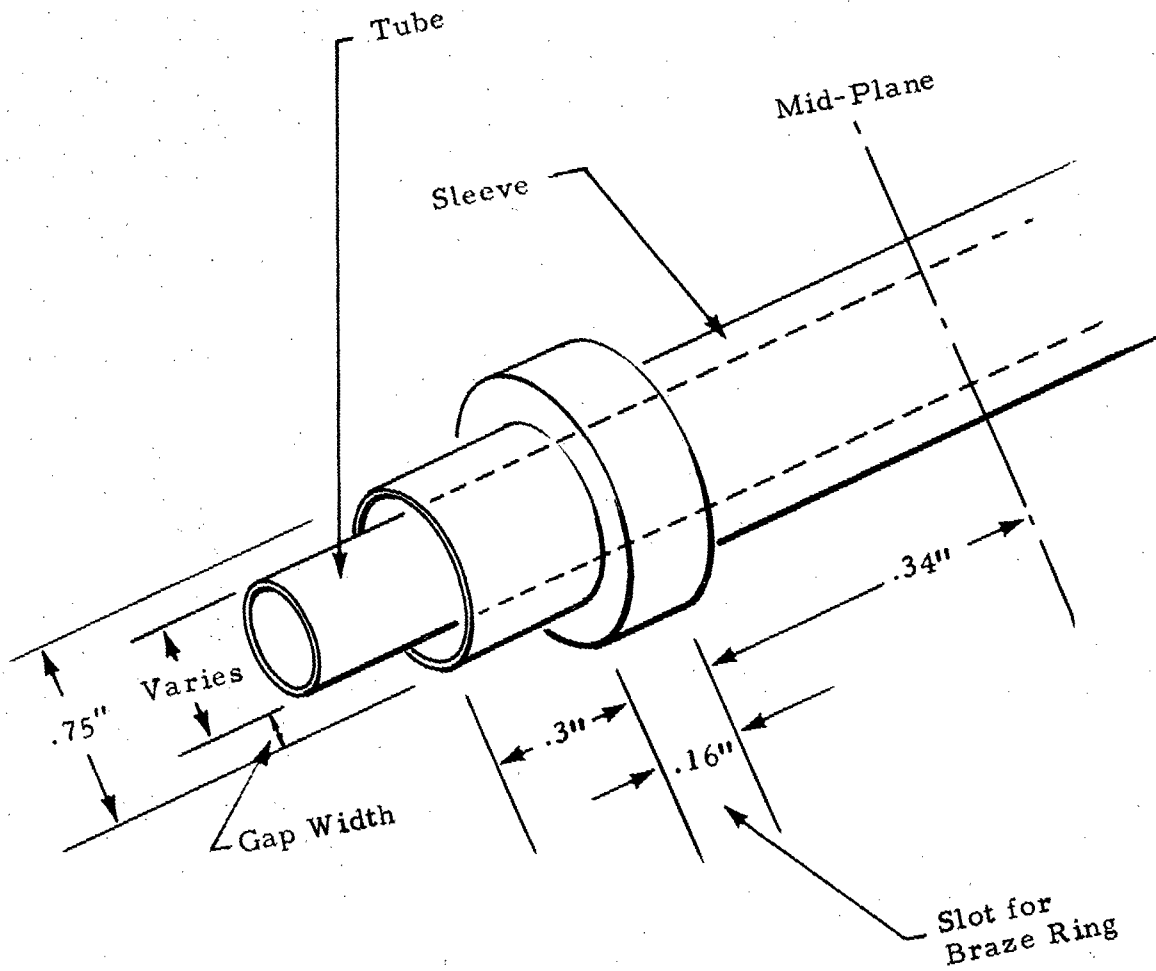


Fig. C-1 - M552 Configuration

$$\phi = \frac{1-k^4}{1-k^2} + \frac{1-k^2}{\ln k}$$

g = gravity

$$h_o = \frac{2\sigma \cos \theta}{\rho g R (1-k)}$$

σ = surface tension

θ = contact angle

Equation (C.1) was developed assuming laminar, steady state, incompressible, isothermal flow with \vec{g} opposing the flow direction. It should be a valid approximation for the M552 configuration and processing conditions.

For very narrow gaps, Eq. (C.1) reduces to that for flow in a slot which is given by

$$u = \frac{\rho g D^2}{12\mu h} (h_o - h) \quad (C.2)$$

where

D = slot width

This equation was developed for assumptions similar to those of Eq. (C.1) and will be just as rigorous except for geometrical effects.

The spreading time, t, for flow in an annulus can be given by

$$t = \frac{-8\mu}{\rho g R^2 \phi} (h_o \ln(1 - h/h_o) + h) \quad (C.3)$$

Again, this equation is valid for isothermal, laminar, incompressible flow with \vec{g} opposing flow. Levich (Ref. C.1) states it will only be an approximation if $t < \frac{\rho R^2}{\mu}$.

The Reynolds number for flow in an annulus is given as (Ref. C-2),

$$Re_1 = \frac{2R(1-k)u\rho}{\mu} \quad (C.4)$$

or by (Ref. C-3),

$$Re_2 = \frac{4R_H u \rho}{\mu} \quad (C.5)$$

where R_H = hydraulic radius.

The transition from laminar to turbulent flow occurs at $Re_2 \approx 2300$. The transition from laminar viscous flow to oscillatory flow is given by $Re_2 = 700$. By making the transformation, $k = 1 - \epsilon$, and allowing $\epsilon \rightarrow 0$, it can be shown that $Re_1 \rightarrow Re_2$ as $k \rightarrow 1$. Thus the transition points for Re_1 are approximately 700 and 2300 also. The Reynolds number for flow in a slot is defined as

$$Re_s = \frac{\rho u D}{\mu}$$

and the laminar-turbulent transition is at $Re_s \approx 2000$.

C.2 M552 BUBBLE DYNAMICS

Many ground and KC-135 aircraft tests for M552 have exhibited a bubble or void space within the braze structure. Analysis of the movement of such a bubble or void in low gravity and the nonisothermal conditions of M552 has been initiated.

Neglecting wall effects, the limiting velocity of a single bubble moving in a homogenous liquid under the combined influence of a gravity field and a temperature gradient is given by Ref. C-4,

$$u = \frac{2}{3 \mu_g B} \left[3 \mu_g a A \frac{d\sigma}{dT} \frac{dT}{dz} - (\rho_g - \rho_l) g a^2 (\mu_g + \mu_l) \right]$$

where

- $A = 2 + k_l/k_g$
- $B = 3 \mu_g + 2 \mu_l$
- $k =$ thermal conductivity
- $\mu =$ viscosity
- $a =$ bubble radius
- $\sigma =$ surface tension
- $T =$ temperature
- $\rho =$ density
- $g =$ gravity

and subscripts l and g refer to the liquid and gas phases, respectively. The temperature gradient affects bubble motion through tangential stresses at the bubble-liquid interface. These stresses are caused by surface tension gradients across the bubble. The surface tension mechanism is termed the Marangoni effect, which can be caused by either temperature or concentration gradients.

The ratio of buoyant/Marangoni forces on the bubble is given by,

$$\gamma = \frac{(\rho_l - \rho_g) g a (\mu_g + \mu_l) A}{3 \mu_g \frac{d\sigma}{dT} \frac{dT}{dz}}$$

where $\gamma =$ buoyancy/surface tension forces. Values of γ for various size bubbles and gravity levels are given below for M552 conditions using a $10^\circ\text{C}/\text{cm}$ temperature gradient,

Bubble Diameter (cm)	Gravity (g/g _E)	γ
10^{-4}	1	10^6
10^{-4}	10^{-6}	1
10^{-2}	1	10^5
10^{-2}	10^{-6}	10^{-1}

Thus, Marangoni forces will be important in Skylab, but not on ground tests.

REFERENCES

- C-1. Levich, V.G., Physicochemical Hydrodynamics, Prentice-Hall, Englewood Cliffs, N.J., 1962.
- C-2. Bird, R.B., W.E. Stewart and E.N. Lightfoot, Transport Phenomena, Wiley, New York, 1960, p. 54.
- C-3. Prengle, R.S., and R.R. Rothfus, Ind. Eng. Chem., Vol. 47, 1955, p. 379.
- C-4. Young, N.O., J.S. Goldstein and M.J. Block, "The Motion of Bubbles in a Vertical Temperature Gradient," J. Fluid Mech., Vol. 6, 1959, p. 356.

Appendix D
DETAILED ANALYSES FOR THE M553
EXPERIMENT

Appendix D

This appendix contains detailed results of calculations for the M553 experiment which were performed during the Phase B portion of this study. The first section of this appendix contains analyses of the driving forces, magnitude and pattern of natural convective fluid flows which occur in the Sphere Forming Experiment. Following sections address such topics as: simple thermal analyses; vaporization; and molten pool splattering due to the impinging electron beam.

D.1 CONVECTION ANALYSIS

As in the other M512 experiments, the fluid dynamics of the M553 experiment is an important factor in determining the quality of the final product. Flow patterns in the molten material are important because all of the sample materials have low entropies of fusion (Ref. D-1). Thus, their solidification (microstructure) is controlled by the rate of heat transfer removal (Ref. D-2), which changes with the fluid flow (Refs. D-3 and D-4). The degree of flow will also determine the amount of mixing attained. If no or little flow were present, all heavier components would segregate to the lower portion of the spheres on earth, but to a negligible extent in the microgravity environment of space. Fluid flow can also affect the shape and release of the specimen while it is retained on the ceramic holder.

Application of dimensional analysis (Refs. D-5 and D-6) to the governing equations for EB melting, coupled with ground-based and KC-135 experiments, should enable prediction of the extent of reduction or increase of motion in the molten metal and/or the change in flow pattern in electron beam melting in space. Possible physical forces which could induce fluid flow in the M553 experiment, and their causes, include:

- Effective Gravity Force: Resultant force on weld specimen due to earth's gravity and centrifugal and coriolis forces of orbiting spacecraft
- Lorentz Force: Electromagnetic forces induced by passage of the electron beam current through the specimen
- Electrostriction: Stresses induced when electrical permittivity changes with density
- Magnetostriction: Stresses induced when permeability changes with density
- Electrostatic Force: Caused by presence of excess electrical charge (due to beam current and/or thermionic emission)
- Surface Tension: Tangential stresses at vapor-liquid interfaces can be induced if surface tension depends on temperature and/or concentration. Surface tension will also cause pressure gradients across curved interfaces.
- Density Differences Accompanying Phase Changes
- Beam Force: Impinging electrons give up their momentum
- Thermal Expansion: Dilation and compression of fluids whose density changes appreciably with temperature can induce fluid flow
- Vibration: Uncontrolled movement due to engine operation, astronaut motion, particle impacts, etc.
- Centrifugal and Coriolis: Generated by disk rotation
- Vapor Pressure: Evaporating molecules impart momentum which leads to normal stresses at vapor-liquid interface.
- Inertia Forces: Tend to sustain induced motions
- Viscous Forces: Tend to resist driving forces.

D.1.1 Governing Equations

The preceding forces, which could influence fluid flow and solidification, appear explicitly in the following conservation equations which apply to formation of a molten pool by electron beam heating.

Continuity (Mass Balance):

$$\frac{\partial \rho}{\partial t} + \nabla \cdot (\rho \vec{V}) = 0$$

where

ρ = density
 \vec{V} = velocity vector
 t = time
 ∇ = "grad" or "del" operator

Momentum:

$$\rho \frac{\partial \vec{V}}{\partial t} + \rho (\vec{V} \cdot \nabla) \vec{V} = -\nabla P + \mu \nabla^2 \vec{V} + \rho \vec{g} + \vec{J} \times \vec{B} + \rho_e \vec{E}$$

Inertia Force
Viscous Force
Gravity Force

Lorentz and Electro-magnetostriction Forces
Electrostatic Force

where

P = pressure
 μ = viscosity
 \vec{g} = gravity vector
 \vec{J} = electrical current density
 \vec{B} = magnetic flux density
 ρ_e = excess charge density
 \vec{E} = electric field density

Energy:

$$\rho C_V \frac{\partial T}{\partial t} + \rho C_V (\vec{V} \cdot \nabla) T = k \nabla^2 T + \Phi + \rho Q$$

$$+ J_c^2 / \sigma' - (\beta T / K) \nabla \cdot \vec{V}$$

Thermal Expansion
Source

where

- T = temperature
 C_V = heat capacity
 k = thermal conductivity
 Φ = viscous dissipation function
 Q = internal heat sources
 J_c = "conduction" current = $\sigma(\vec{E} + \vec{V} \times \vec{B})$
 σ' = electrical conductivity
 $\beta = -\frac{1}{\rho} \left(\frac{\partial \rho}{\partial T} \right)_P$
 $K = \frac{1}{\rho} \left(\frac{\partial \rho}{\partial P} \right)_T$

Maxwell's Equations:

$$\nabla \times \vec{E} = - \partial \vec{B} / \partial t$$

$$\nabla \times \vec{H} = \vec{J} + \partial \vec{D} / \partial t$$

$$\nabla \cdot \vec{B} = 0$$

$$\nabla \cdot \vec{D} = \rho_e$$

where

- \vec{D} = displacement current
 \vec{H} = Magnetic flux

Constitutive Relations:

$$\begin{aligned}\vec{D} &= \epsilon' \vec{E} \\ \vec{B} &= \mu' \vec{H} \\ \vec{J} &= \sigma'(\vec{E} + \vec{V} \times \vec{B}) + \rho_e \vec{V} \\ \rho &= \rho_o \left[1 - \beta \Delta T + K \Delta P \right]\end{aligned}$$

where

ϵ' = permittivity (dielectric constant)

μ' = permeability

Vapor-Liquid Boundary Conditions:

Force Balance,

$$\begin{aligned}& \underbrace{\left[P^{(2)} - P^{(1)} \right] n_i}_{\text{Beam and Vapor Pressure Forces}} + \underbrace{\frac{\partial S}{\partial X_i} + S \left[\frac{1}{R_1} + \frac{1}{R_2} \right] n_i}_{\text{Surface Tension Forces}} \\ &= \left[\mu^{(2)} \left(\frac{\partial v_i^{(2)}}{\partial X_k} + \frac{\partial v_k^{(2)}}{\partial X_i} \right) - \mu^{(1)} \left(\frac{\partial v_i^{(1)}}{\partial X_k} + \frac{\partial v_k^{(1)}}{\partial X_i} \right) \right] n_k\end{aligned}$$

where $P^{(1,2)}$, $\mu^{(1,2)}$, $v_i^{(1,2)}$, $v_k^{(1,2)}$ are, respectively, the pressures, viscosities, and velocity components in Phases 1 and 2, S is the surface tension, R_1 and R_2 are the principal radii of curvature of the surface, n_i ($i=1,2,3$) are the components of the unit vector normal to the surface and directed into the interior of Phase 1, and summation over a repeated index ($k=1,2,3$) is assumed.

Energy Balance,

$$\epsilon \sigma (T_s^4 - T_\infty^4) - k \vec{n} \cdot \nabla T_s = Q_{EB}$$

where

- ϵ = emissivity
- σ = Boltzmann's constant
- T_s = surface temperature
- T_∞ = environment temperature
- \vec{n} = outward unit normal vector to free surface
- Q_{EB} = heat flux from electron beam

Continuity of Velocity,

$$\vec{n} \times (\vec{V}^{(1)} - \vec{V}^{(2)}) = 0$$

$$\vec{n} \cdot \vec{V}^{(1)} = \vec{n} \cdot \vec{V}^{(2)} = 0$$

Solid-Liquid Boundary Conditions:

Along stationary interfaces the no-slip condition (all components of velocity vanish) holds; whereas at moving interfaces (along melting or freezing fronts), a one-dimensional material balance yields

$$u_i = (1 - \rho_s/\rho_L) d\delta/dt$$

where

- u_i = fluid velocity normal to the interface
- δ = position of the interface relative to the origin of the spatial coordinate system
- ρ_s = solid density
- ρ_L = liquid density

This is the source of the density-difference-accompanying-phase-change force for fluid flow. Also for a melting interface, an energy balance yields:

$$-k\nabla (T_L - T_S) = \rho_s \lambda \frac{d\delta}{dt}$$

where

T_L = liquid temperature at the interface

T_S = solid temperature at the interface

λ = heat of fusion

and

$$T_S = T_L$$

The preceding equations are based on the following assumptions:

- No influence of external fields on physical properties
- No coupling between constitutive flux relations (e.g., no Soret effect)
- Single-component, Newtonian fluid
- Constant physical properties
- Bulk coefficient of viscosity vanishes.

They are written in general vector form wherever possible, since they also apply directly to M551. It should be noted that only the differences in physical properties and geometry will differ in a dimensional analysis of M551 versus M553.

D.1.2 Dimensional Analysis

The controlling physical forces can be determined by nondimensioning each of the preceding equations and performing an order-of-magnitude comparison on the various dimensionless groups which result (Refs. D-5 and D-6).

The key to successful analysis is in choosing the proper reference values; i.e., since no freestream velocity exists, which forces do we equate to estimate a "characteristic" or "typical" velocity. Choosing the proper characteristic velocity is very important, since the reference time, temperature, etc. usually depend on this velocity.

Previous examinations of film showing both KC-135 flight experiments and ground tests for the M553 experiment indicated fluid velocities exceeded 300 cm/sec (p. B-5 of Ref. D-7). Continued M553 film analysis has since shown that flow velocities for nickel specimens on both KC-135 and ground tests have been approximately 20 cm/sec. Of the 14 possible forces affecting electron beam melting (Ref. D-8), only those shown in Table D-1 yield characteristic velocities of this order of magnitude. These driving forces consist of couplings involving surface tension, gravity of Lorentz (electromagnetic) forces with inertia forces. Previous studies based on faster velocities had indicated coupling with viscous, rather than inertia, forces as controlling (Ref. D-7). This indicates the importance of choosing the correct characteristic velocity. Preliminary analysis also suggests that magnetostriction forces may also be important, but gross uncertainty in electromagnetic property data for liquid metals precludes any decision at the present time.

The dimensionless momentum equation which determines fluid flow in electron beam melting becomes (upon choosing the surface tension-inertia characteristic velocity),

$$\frac{1}{N_{St}} \rho \frac{\partial \bar{V}}{\partial t} + \frac{1}{N_{Oh}} \rho (\bar{V} \cdot \nabla) \bar{V} = - \frac{1}{2N_{Oh}} \nabla P + \nabla^2 \bar{V} + \frac{N_{Bo}}{N_{Oh}} (\rho \bar{g}) + \frac{2N_{MI}}{N_{Oh}} (\bar{V} \times \bar{B}) \times \bar{B} \quad (D.1)$$

where

$$\begin{aligned} N_{St} &= \text{Stokes number} = \mu t_o / \rho_o L \\ &= \text{duration of process / residence time} \end{aligned}$$

Table D-1
 PROBABLE CHARACTERISTIC VELOCITIES
 IN ELECTRON BEAM MELTING

Controlling Forces	Velocity	
	Functional Form	Value (cm/sec) for Nickel in M553
Inertia = Surface Tension	$(ST/\rho L)^{1/2}$	20
Inertia = Lorentz	$(\sigma^2 E^2 L/\rho)^{1/3}$	1
Inertia = Gravity	$(gL)^{1/2}$	18 at $1 g_E$ 6 at $10^{-4} g_E$
Viscous = Lorentz	$(\sigma^2 E^2 L^2/\mu)^{1/2}$	7

$$N_{Oh} = \text{Ohnsorge number} = \mu / \sqrt{\rho_o L S T_o}$$

$$= \text{viscous force/surface tension force}$$

$$N_{Bo} = \text{Bond number} = \rho_o g_o L^2 / S T_o$$

$$= \text{gravity force/surface tension}$$

$$N_{MI} = \text{Magnetic interaction number} = \frac{B_o^2 L}{2 \mu_o' S T_o}$$

$$= \text{magnetic force/surface tension}$$

Using physical property data for nickel and beam parameters for the M553 experiment, the equation reduces to

$$10^3 \rho \frac{\partial \bar{V}}{\partial t} + 10^3 \rho (\bar{V} \cdot \nabla) \bar{V} = -10^3 \nabla P + \nabla^2 \bar{V} + G(\rho \bar{g}) + 10^{-1} (\nabla \times \bar{B}) \times \bar{B}$$

where

$$G = 10^3 \text{ for earth gravity}$$

$$G = 10^{-1} \text{ for expected Skylab gravity.}$$

This order-of-magnitude analysis indicates that surface tension driven convection will occur both in ground tests and for Skylab conditions because $N_{Oh} \ll 1$. This is confirmed by KC-135 M553 tests. Furthermore, gravity driven convection will exist on ground tests, but will be negligible in the reduced gravity of Skylab. Thus different forces will control convection on earth versus Skylab. The preceding analysis also indicates that electromagnetic or Lorentz forces will be negligible with regard to causing fluid motion.

The surface tension driving force considered above is actually a surface tension gradient caused by radial and lateral temperature gradients. Ignoring convection, gradients of at least several hundred degrees Celsius per centimeter have been predicted during melting (Ref. D-9). It can be shown by dimensional analysis (equate inertial and viscous terms) that the motion

caused by the initial temperature gradients will occur in less than 0.1 second and can persist for 60 seconds after removing the driving force. This means that there will be some fluid motion during solidification if the M553 specimens freeze after 30 to 40 seconds as predicted.

Values of the pertinent dimensionless groups for the remaining M553 materials are given in Table D-2. As can be seen, no significant changes are evident from the preceding conclusions for pure nickel.

It should also be mentioned that the effects on fluid motion of surface free charges (excess electrostatic charge) and related electric and magnetic forces at the drop surfaces have been examined. The results of the examination indicate that these surface charges are negligible driving forces for fluid motion. These results were also reviewed by Professor J. R. Melcher of MIT's Electrical Engineering Department, and he was in full agreement with these results (Ref. D-10). Furthermore, from the manner in which patches of surface contaminants moved about in the ground films, it is apparent that surface tension driven flows due to concentration gradients are also important in this experiment. No reliable data exist, however, on what these impurities are, nor what the value of surface tension gradient with composition is. Thus the Marangoni effects are limited to thermal differences only in this study.

D.1.3 Flow Patterns

The aforementioned difference in controlling forces between terrestrial and space processing of the M553 experiment should result in altered flow patterns between these two conditions. From a knowledge of flow patterns generated by surface tension versus buoyancy controlled natural convection on Earth, the situation illustrated in Fig. D-1 would no doubt exist during melting on Earth, while that shown in Fig. D-2 would prevail in space.

The patterns shown in Fig. D-2 are based on the fact that surface tension is stronger in cooler regions; therefore the coolest portion of the specimen will exert the strongest "pull" on the surface. The buoyancy modification

Table D-2
M553 DIMENSIONAL ANALYSIS

Material	N_{Oh}	N_{Bo}	$\frac{1}{N_{Oh}}$	$\frac{N_{Bo}^*}{N_{Oh}}$	$\frac{N_{Bo}^\dagger}{N_{Oh}}$
Ni-Sn	4.4×10^{-4}	1.50	2292	3437	.34
Ni-Ag	5.0×10^{-4}	1.53	1991	3043	.30
Ni-Cu	4.45×10^{-4}	1.54	2107	3241	.32

* With Earth gravity (9.8 m/sec^2)

† With 10^{-4} Earth gravity

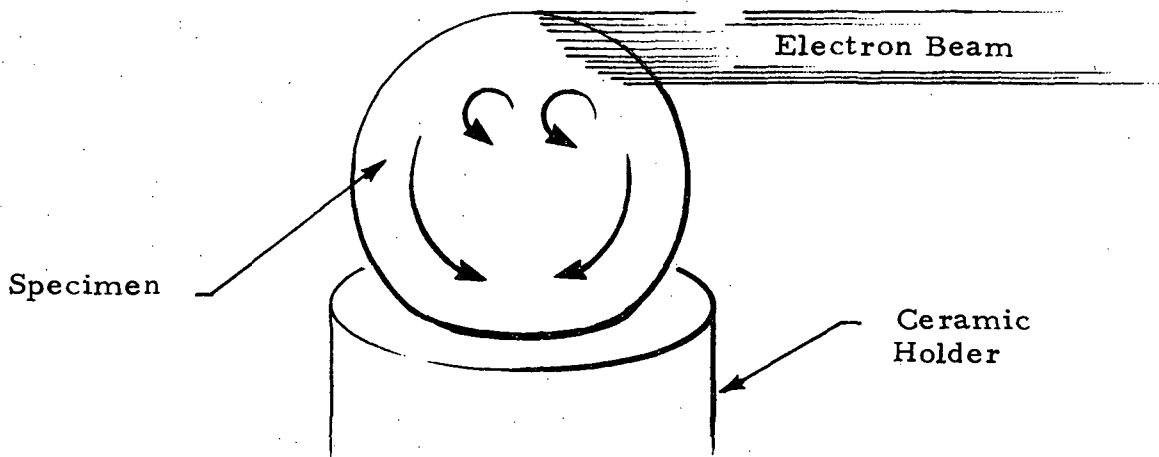


Fig. D-1 - Convective Patterns in the M553 Specimen During Melting on Earth

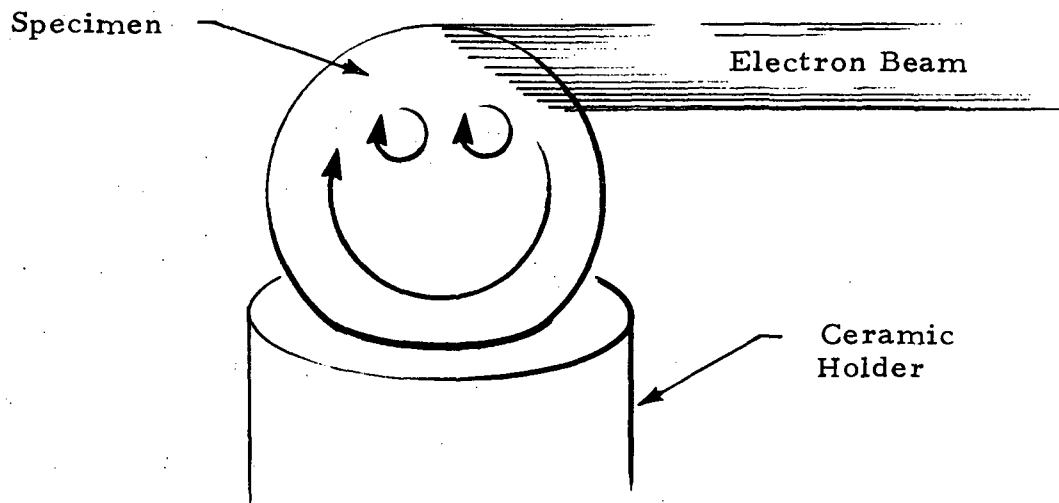


Fig. D-2 - Convective Patterns in the M553 Specimen During Melting in Space

exhibited in Fig. D-1 reflects the rise of warmer portions of fluid in a gravity field coupled with surface tension flows.

D.2 M553 THERMAL ANALYSIS

A critical question which must be answered for the M553 experiment is, "How long will it take for the released specimens to cool down to a "touch" temperature of 105°F?" Two separate models were formulated to study this problem. The results are shown in Table D-3. These results were based on the specimens being at the melting point (no superheat) upon release.

Specimen conditions reported in Table D-3 include: free floating in vacuum; free floating and chamber backfilled with cabin atmosphere (5 psi mixture of 70% O₂ and 30% N₂) two minutes after specimen release; and free-floating specimen and the chamber pumped with a steady stream of cabin atmosphere at a flow rate of 5 cu ft/min. In the last case, the flow is considered to start two minutes after specimen release.

Results shown in Table D-3 indicate that the chamber will be safe to open eight minutes after release of the last M553 specimen if a cabin atmosphere flow of 5 cu ft/min is established within the chamber two minutes after release of this last specimen. Otherwise, up to several hours may be needed for specimen cooldown to touch temperature. If the chamber is backfilled with 5 psi cabin atmosphere, cooldown time is roughly 35 to 40 minutes with 5 psi air versus several hours, unless the spheres remain attached to the chamber walls. It is unlikely, however, that all 11 of the released specimens will remain attached to a solid surface.

The first model formulated was for a free-floating sphere being cooled by conduction and convection to an ambient atmosphere and/or being cooled by radiation to the chamber walls. Assuming that only sensible heat is being removed (no phase change) and that thermal diffusivity is infinitely large (an extremely good conductor), the energy balance becomes

Table D-3
M553 COOLDOWN TIMES

Thermal Condition of Specimen	Cooldown Time*	Chamber Wall Temperature ($^{\circ}$ F)
Free floating in vacuum	3.3 hr	80
	2.6 hr	60
	2.5 hr	-460
Sticks to wall	6 sec	80
Sticks to wall for 0.5 sec	3.3 hr	80
Free floating and chamber backfilled with 5 psi mixture of 70% O ₂ and 30% N ₂	34 min	80
Free floating and 5 psi, 70% O ₂ - 30% N ₂ cabin air flow at 5 cu ft/min through chamber	7.7 min	80

* For individual 0.25 in. molten nickel spheres at their melting point to reach 105 $^{\circ}$ F.

$$\rho V C \frac{\partial T}{\partial t} = -A \sigma \epsilon (T^4 - T_w^4) - A h (T - T_o) \quad (D.2)$$

where

- T = sphere temperature
- T_w = wall temperature
- T_o = chamber atmosphere temperature ($\approx T_w$)
- σ = Boltzmann's constant
- ϵ = emissivity of sphere
- h = convective heat transfer coefficient
- A = surface area of specimen
- ρ = specimen density
- V = volume of specimen
- C = heat capacity of specimen
- t = time

The coefficient h, for stationary cabin atmosphere, can be estimated by Ref. D-11.

$$h = \frac{k}{D} (2 + Gr^{1/4} Pr^{1/3})$$

where

- k = thermal conductivity
- D = sphere diameter
- Gr = Grashof number
- Pr = Prandtl number

For the condition of cabin air through the chamber, the heat transfer coefficient for the sphere (forced convection cooling of small spheres) can be obtained from a plot of Nusselt number versus Reynolds number and Prandtl number given in Ref. D-11.

Equation (D.2) is valid for either a molten or solidified specimen. A computer program written in FORTRAN IV was written to solve Eq. (D.2) utilizing a fourth-order Runge-Kutta numerical algorithm. The output of this program is a temperature versus time profile.

An estimate of the freezing time, t_f , for this model, again assuming infinite thermal diffusivity is given by

$$t_f = \frac{\rho R \lambda}{3 \left[\epsilon \sigma T^4 - h (T - T_w) \right]} \quad (D.3)$$

A correction time, t_c , for the effect of finite thermal conductivity is given by

$$t_c = \rho C R^2 / k \quad (D.4)$$

Thus the time for a molten, free-floating specimen at its melting point to cool down to touch temperature is given by

$$t_T = t_f + t_s + t_c$$

where

t_T = total time to reach touch temperature

t_s = time to remove sensible heat (from Eq. (D.2))

The second model was developed for a specimen attached to the chamber wall being cooled by conduction to the wall and radiation. The chamber atmosphere was assumed to be a hard vacuum. Again, assuming that only sensible heat is being removed and that the specimen is a perfect conductor, the energy balance becomes,

$$\rho V C \frac{\partial T}{\partial t} = -A' \epsilon \sigma (T^4 - T_w^4) - A_w h_e (T - T_w) \quad (D.5)$$

where

A_w = contact area between the specimen and chamber wall

A' = free surface area of specimen

h_e = effective heat transfer coefficient to account for conduction losses

Over the area of contact, A_w , the chamber wall can be assumed to be flat, therefore A_w and A' can be derived using simple geometry and are given by

$$A_w = \frac{\pi^{1/3} \sin^2 \theta V^{2/3}}{(1 - \cos \theta)^{4/3} \left(\frac{2 + \cos \theta}{3} \right)^{2/3}}$$

$$A' = 2 \left(\frac{1 - \cos \theta}{\sin^2 \theta} \right) A_w$$

where

θ = contact angle.

The effective transfer coefficient is given by

$$h_e = k_w / L$$

where

k_w = thermal conductivity of chamber wall

L = some characteristic length for conduction in the wall.

The characteristic length L can be estimated by

$$L = D k_w / 2k$$

The freezing time and correction time for finite conductivity can be estimated from Eqs. (D.3) and (D.4), respectively.

Equation (D.5) can be solved using the algorithm developed for Eq. (D.2).

D.3 VAPORIZATION IN M553

A brief study of vaporization losses expected for nickel, aluminum, copper and silver under conditions expected during the melting portion of the M553 experiment indicates that aluminum will evaporate 50 times faster than nickel, 25 times faster than silver and 10 times faster than copper. Thus, Ni-Al(5%) should not be considered as a material in the sphere forming experiment. The effect of concentration was included and the other sample materials were thus Ni-Ag(1%), Ni-Cu(30%), and pure nickel.

The above data were obtained using Langmuir's formula

$$\dot{m} = P_v \sqrt{\frac{M}{2\pi RT}} \text{ kg/m}^2\text{-sec}$$

where

- \dot{m} = vaporization rate
- M = molecular weight
- P_v = partial pressure
- T = surface temperature
- R = gas constant

Surface temperatures were conservatively estimated to be 1725°K.

D.4 MELT SPLATTERING INSTABILITY

In both the M551 and M553 experiments, the heat released to the metal specimens by the impinging electron beam enables a molten pool to form. A question arises as to the stability of these molten liquids in low gravity. At

least one of the KC-135 M553 specimens was seen to break up violently into many smaller liquid spheroids upon complete melting. The electron beam was still hitting the specimen during break up. A similar instability might develop in the molten puddle formed during the dwell mode of the M551 experiment, wherein the liquid might not adhere and separate from the solid disk (violent splattering).

There are at least three different mechanisms which might explain the instability observed in the M553 KC-135 specimens. Upon melting, the specimen may have experienced violent degassing which could have led to droplet breakup. Another mechanism might be electrohydrodynamic instability caused by interactions between the electromagnetic forces for the electron beam and the fluid flow field set up in the molten metal by both thermal gradients, Lorentz and other forces. Lastly, the momentum force associated with the impinging electron beam might have set up unstable surface oscillations on the molten metal.

The latter instability mechanism has been treated recently by Berghmans (Ref. D-12). He performed a theoretical study of fluid interface stability with special attention being given to the role of surface tension. A detailed examination of this instability mechanism for both the M551 and M553 experiments is given in Appendix B where it is shown that the electron beam momentum force is not the cause of splattering in either of these experiments.

REFERENCES

- D-1. Laudise, R. A., J. R. Carruthers, and K. A. Jackson, "Crystal Growth," in Annual Review of Materials Science, Vol. 1, 1971, pp. 253-256.
- D-2. Laudise, R. A., The Growth of Single Crystals, Prentice, Hall, Englewood Cliffs, N. J., 1970, pp. 86-103.
- D-3. Goldak, J. A., G. Burbidge and M. J. Bibby, "Predicting Microstructure from Heat Flow Calculations in Electron Beam Welded Eutectoid Steels," Can. Met. Quart., Vol. 9, 1970, p. 459.
- D-4. Cole, G. S., "Transport Processes and Fluid Flow in Solidification," in Solidification, American Society for Metals, Metals Park, Ohio, 1971, pp. 201-274.
- D-5. Churchill, S. W., and J. D. Hellums, "Dimensional Analysis and Natural Convection," Chem. Engr. Prog. Symp. Ser., Vol. 57, 1964, p. 75.
- D-6. Ostrach, S., "Role of Analysis in the Solution of Complex Problems," Third Intl. Heat Trans. Conf. , Chicago, August 1966.
- D-7. Lockheed Missiles & Space Company, "Convection in Space Processing - Bimonthly Progress Report," LMSC-HREC D306308, 5 December 1972, pp. B-1 through B-12.
- D-8. Lockheed Missiles & Space Company, "Convection in Space Processing - Bimonthly Progress Report," LMSC-HREC D306219, 28 September 1972, p. B-9.
- D-9. Lockheed Missiles & Space Company, "Research Study on Materials Processing in Space Experiment M512 - Monthly Progress Report," LMSC-HREC PR D306549, Huntsville, Ala., 28 March 1973.
- D-10. Melcher, J. R., discussions on Electrohydrodynamic Applications in Space Processing, Marshall Space Flight Center, Huntsville, Ala., 11 June 1973.
- D-11. Bird, R. B., W. E. Stewart and E. N. Lightfoot, Transport Phenomena, Wiley, New York, 1960, p. 413.
- D-12. Berghmans, J., "Theoretical Investigation of the Interfacial Stability of Inviscid Fluids in Motion, Considering Surface Tension," J. Fluid Mech., Vol. 54, 1972, pp. 129-141.